

Kondo and Majorana signatures near the singlet-doublet quantum phase transition

G. Górski,¹ J. Barański,² I. Weymann,³ and T. Domański^{4,*}

¹*Faculty of Mathematics and Natural Sciences, University of Rzeszów, 35-310 Rzeszów, Poland*

²*Institute of Physics, Polish Academy of Sciences, 02-668 Warsaw, Poland*

³*Faculty of Physics, A. Mickiewicz University, 61-614 Poznań, Poland*

⁴*Institute of Physics, M. Curie-Skłodowska University, 20-031 Lublin, Poland*

(Dated: March 8, 2024)

We study the low energy spectrum of a correlated quantum dot embedded between the normal conducting and superconducting reservoirs and hybridized with the topological superconducting nanowire, hosting the Majorana end-modes. We investigate the leaking Majorana quasiparticle and inspect its interplay with the proximity induced on-dot pairing and correlations. In particular, we focus on the subgap Kondo effect near the quantum phase transition/crossover from the spinfull (doublet) to the spinless (BCS-type singlet) configurations. Treating the correlations perturbatively and within the NRG approach we study its signatures observable in the Andreev (particle-to-hole conversion) tunneling spectroscopy. We find, that the leaking Majorana mode has a spin-selective influence on the subgap Kondo effect.

I. INTRODUCTION

Intensive studies have been recently devoted to quasiparticles, resembling the Majorana fermions [1–7] that are identical with their own antiparticles. These exotic objects have been predicted at defects [8] or boundaries of topological superconductors [9, 10] and their non-Abelian character make them appealing for quantum computing or novel spintronic devices [11]. Majorana quasiparticles have been predicted in various setups [12–22], but their experimental realization has been so far reported only in the ballistic tunneling [23, 24] and STM measurements [25–28] through the nanowires proximity-coupled to the bulk *s*-wave superconductors.

Inspired by the work by M.T. Deng *et al.* [29], who provided experimental evidence for the Majorana mode leaking into the quantum dot side-attached to InAs nanowire, we propose here a slightly different setup (Fig. 1) for studying interplay between: electron pairing and the Kondo effect in presence of the Majorana quasiparticle. Leakage of such mode has been initially predicted by E. Vernek *et al.* [30]. Coalescence of the Andreev states into the zero-energy Majorana state has been thoroughly discussed by various groups [31–33], addressing also correlation effects on the Hartree-Fock level [34], within the equation of motion approach [35], and using NRG [36] (but for very weak coupling Γ_N to the conducting lead). Our present study is complementary to the former analysis, focusing on the subgap Kondo effect driven by an effective exchange interaction of the correlated quantum dot with the normal lead [37, 38]. Such situation could be realized in STM-type geometry, similar to what has been used by the Princeton [25] and Basel [26] groups. For instance, one can use a nanoscopic Fe chain with one (or a few) side-coupled nonmagnetic atoms (like Ag or Au) deposited on the superconducting substrate (e.g.

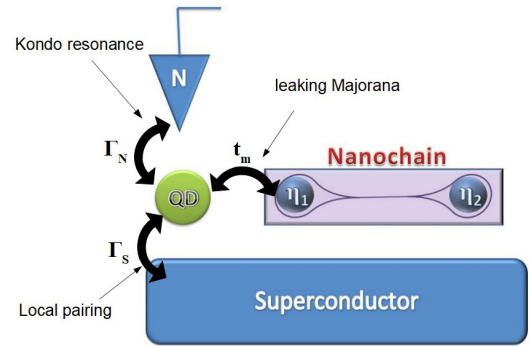


FIG. 1. Scheme of the quantum dot (QD) deposited on superconducting substrate (S) and hybridized with the Rashba nanowire [hosting the Majorana end-modes η_1 and η_2] which is probed by the metallic tip (N) via the Andreev tunneling.

Pb or Al) and probe it either by the normal [25, 26] or ferromagnetic [28] STM tip.

The quantum dot (QD) embedded between a superconducting (S) and metallic (N) leads and side-coupled to the Majorana nanowire (Fig. 1) is formally affected by three reservoirs. We assume, however, that charge tunneling occurs only via metallic tip – quantum dot – superconductor circuit. In other words, the nanowire plays here a role of ‘floating’ lead. Without the Majorana mode a relationship between the subgap Kondo effect and the on-dot pairing has been analyzed for N-QD-S setup by several authors [37–39]. Here we extend this analysis, considering influence of the Majorana mode on the low-energy (subgap) electronic states. We study the resulting spectroscopic signatures, focusing on the quantum phase transition/crossover from the spinfull (singly occupied) to the spinless (BCS-type) configurations [37, 38].

Correlations and the Majorana mode have been already studied for QD embedded between the metallic [30, 40–47] or ferromagnetic [48, 49] electrodes. It has been shown, that the leaking Majorana quasiparticle affects the Kondo resonance of such ‘normal’ QD and its

* e-mail: doman@kft.umcs.lublin.pl

signatures are observable in the linear conductance. In particular, for the long nanowires (with negligible overlap between Majorana modes) the linear conductance reaches $3e^2/2h$, whereas for the short ones (with the overlapping Majoranas) the conductance reaches $2e^2/h$ [41, 42, 48, 49]. Analysis of the thermoelectric properties of such N-QD-N setup has revealed that for small overlap the thermopower would reverse its sign [41, 48, 49].

For junctions, comprising the normal and superconducting electrodes a relationship between the Majorana quasiparticle with the subgap Kondo effect is much less explored [35, 36, 44, 50]. Through the proximity effect, the QD acquires pairing [51, 52] thereby all processes engaging a given spin simultaneously affect its opposite counter-partner [53]. In such situation, the Majorana quasiparticle hybridized with, let's say \uparrow electron, would affect the spectrum of \downarrow electrons. Our present analysis shows, that the leaking Majorana quasiparticle has a *spin-selective influence on the subgap Kondo effect*. Since both spin components are important for the Andreev scattering we discuss in some detail the resulting subgap transport properties.

The paper is organized as follows. In Sec. II we formulate the microscopic model. In Sec. III we study the subgap QD spectrum and the tunneling conductance, neglecting the correlations. Next, in Sec. IV, we consider the correlated QD in the subgap Kondo regime. In Sec. V we summarize the main results. Appendices provide details, concerning influence of the magnetic field, finite polarization of Majorana modes, their overlap, etc.

II. LOW ENERGY MODEL

Empirical realizations of the topological superconductivity in the semiconducting wires [23, 24] or magnetic atoms' chain [25–28] rely on the p -wave pairing (of identical spins) between the nearest neighbor sites, reminiscent of the Kitaev scenario [10]. In this paper we assume that such pairing is induced for \uparrow electrons, so only this particular spin component of QD is *directly* coupled to the Majorana quasiparticle [30, 54]. Due to the proximity induced on-dot pairing, the other (\downarrow) spin is *indirectly* influenced by the Majorana quasiparticle as well. For this reason, any process engaging \uparrow electrons would simultaneously (although with different efficiency) affect the opposite spin [53]. This would be very important for the

Andreev (particle to hole conversion) scattering, which is the only subgap transport channel at low temperatures.

Our setup (Fig. 1) can be described by the following Anderson-type Hamiltonian

$$H = \sum_{\beta=S,N} (H_{\beta} + H_{\beta-QD}) + H_{QD} + H_{MQD}, \quad (1)$$

where $H_N = \sum_{k,\sigma} \xi_{kN} c_{k\sigma N}^{\dagger} c_{k\sigma N}$ describes the metallic electrode, $H_S = \sum_{k,\sigma} \xi_{kS} c_{k\sigma S}^{\dagger} c_{k\sigma S} - \sum_k (\Delta c_{k\uparrow S}^{\dagger} c_{-k\downarrow S}^{\dagger} + h.c.)$ refers to s -wave superconducting substrate and electron energies $\xi_{k\beta}$ are measured with respect to the chemical potentials μ_{β} . The correlated QD is described by $H_{QD} = \sum_{\sigma} \epsilon d_{\sigma}^{\dagger} d_{\sigma} + U n_{\downarrow} n_{\uparrow}$, where ϵ denotes the energy level and U stands for the repulsive interaction between opposite spin electrons. The QD is coupled to both external reservoirs via $H_{\beta-QD} = \sum_{k,\sigma} (V_{k\beta} d_{\sigma}^{\dagger} c_{k\sigma\beta} + h.c.)$, where $V_{k\beta}$ denote the matrix elements. In a wide bandwidth limit, it is convenient to introduce the auxiliary couplings $\Gamma_{\beta} = 2\pi \sum_k |V_{k\beta}|^2 \delta(\omega - \xi_{k\beta})$, which we assume to be constant. It can be shown [55–58], that for $|\omega| \ll \Delta$ the superconducting electrode induces the static pairing $H_S + H_{S-QD} \approx -\frac{\Gamma_S}{2} (d_{\uparrow} d_{\downarrow} + d_{\downarrow}^{\dagger} d_{\uparrow}^{\dagger})$. We make use of this low energy model, whose extension to arbitrary values of Δ has been discussed for instance in Ref. [31].

The zero-energy end modes of the topological nanowire can be modeled by the following term [45]

$$H_{MQD} = i\epsilon_m \eta_1 \eta_2 + \lambda (d_{\uparrow}^{\dagger} \eta_1 + \eta_1 d_{\uparrow}) \quad (2)$$

with the hermitian operators $\eta_i = \eta_i^{\dagger}$, where ϵ_m corresponds to their overlap. We recast these Majorana operators by the standard fermionic ones [5] $\eta_1 = \frac{1}{\sqrt{2}}(f + f^{\dagger})$ and $\eta_2 = \frac{-i}{\sqrt{2}}(f - f^{\dagger})$ so that (2) can be expressed as

$$H_{MQD} = t_m (d_{\uparrow}^{\dagger} - d_{\uparrow})(f + f^{\dagger}) + \epsilon_m f^{\dagger} f - \frac{\epsilon_m}{2}, \quad (3)$$

where $t_m = \lambda/\sqrt{2}$.

III. MAJORANA VS ELECTRON PAIRING

We first consider the case of uncorrelated QD ($U = 0$). Let us calculate the Green's function $\mathcal{G}(\omega) = \langle\langle \Psi; \Psi^{\dagger} \rangle\rangle$ in the following matrix notation $\Psi = (d_{\uparrow}, d_{\downarrow}, f, f^{\dagger})$

$$\lim_{U=0} \mathcal{G}^{-1}(\omega) = \begin{pmatrix} \omega - \epsilon + i\Gamma_N/2 & \Gamma_S/2 & -t_m & -t_m \\ \Gamma_S/2 & \omega + \epsilon + i\Gamma_N/2 & 0 & 0 \\ -t_m & 0 & \omega - \epsilon_m - t_m^2/b & -t_m^2/b \\ -t_m & 0 & -t_m^2/b & \omega + \epsilon_m - t_m^2/b \end{pmatrix}, \quad (4)$$

where $b = \omega + \epsilon + i\Gamma_N/2 - (\Gamma_S/2)^2/(\omega - \epsilon + i\Gamma_N/2)$. For $\epsilon_m = 0$ (i.e. without any overlap between the Majorana

modes) the Green's function (4) simplifies to

$$\mathcal{G}_{11}(\omega) = \frac{\omega + \epsilon + i\frac{\Gamma_N}{2}}{D_1(\omega)} + \frac{2t_m^2(\omega + \epsilon + i\frac{\Gamma_N}{2})^2}{D(\omega)}, \quad (5)$$

$$\mathcal{G}_{22}(\omega) = \frac{\omega - \epsilon + i\frac{\Gamma_N}{2}}{D_1(\omega)} + \frac{2t_m^2(\frac{\Gamma_S}{2})^2}{D(\omega)}, \quad (6)$$

$$D(\omega) = -\frac{\Gamma_S}{2} - 2t_m^2(\omega + \epsilon + i\frac{\Gamma_N}{2})\frac{\Gamma_S}{2}$$

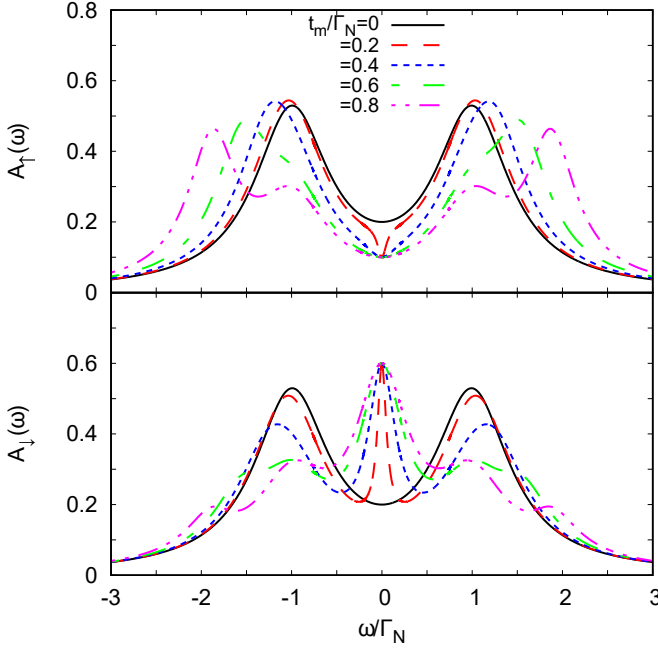


FIG. 2. The normalized spectral function $A_\sigma(\omega) = \frac{\pi}{2}\Gamma_N\rho_\sigma(\omega)$ of the uncorrelated dot $U = 0$ obtained for $\Gamma_S = 2\Gamma_N$, $\epsilon = 0$ and various couplings t_m .

where $D(\omega) \equiv D_1(\omega)[\omega D_1(\omega) - 4t_m^2(\omega + i\Gamma_N/2)]$ and $D_1(\omega) \equiv (\omega + i\Gamma_N/2)^2 - \epsilon^2 - (\Gamma_S/2)^2$. These Green's functions (5)-(7) are composed of the part, representing solution for the quantum dot coupled only to N and S electrodes ($t_m = 0$) (first terms of r.h.s Eqs. (5)-(7)) and additional term dependent on coupling to the Majorana fermions. In the 'superconducting atomic limit' ($\Gamma_N \rightarrow 0$) such Green's function is characterized by five poles: two corresponding to the Andreev bound states ($\pm\sqrt{\epsilon^2 + (\Gamma_S/2)^2}$) and three additional states resulting from the Majorana fermions ($0, \pm\sqrt{\epsilon^2 + (\Gamma_S/2)^2 + (2t_m)^2}$).

A. Free quasiparticle spectrum

Figure 2 shows the spin-resolved normalized spectral function $A_\sigma(\omega) = \frac{\pi}{2}\Gamma_N\rho_\sigma(\omega)$ of the uncorrelated QD obtained at half-filling ($\epsilon = 0$) for various couplings t_m . As a reference shape we also present the spectrum in absence of the Majorana quasiparticles ($t_m = 0$), revealing the Andreev quasiparticle peaks at $\omega = \pm\sqrt{\epsilon^2 + (\Gamma_S/2)^2}$ whose broadening is Γ_N . For $t_m \neq 0$ the spin-resolved spectra are no longer identical due to the direct (indirect) coupling of \uparrow (\downarrow) QD electrons with the side-attached Majorana state. The most significant differences show up near $\omega \sim 0$. In particular, direct hybridization of \uparrow electrons depletes their spectrum near the Majorana state. Exactly at $\omega = 0$ their spectral function is reduced by half, $A_\uparrow(0)|_{t_m \neq 0} = 0.5A_\uparrow(0)|_{t_m=0}$, similarly to what has been reported for the same geometry with both

nonsuperconducting leads [42, 48, 54]. Contrary to this behavior, the spin \downarrow electrons (indirectly coupled to the Majorana state via on-dot pairing) clearly gain the electronic states. Again, at $\omega = 0$ the spectral function $A_\downarrow(0)$ does not depend on t_m (unless t_m vanishes). This constructive feedback of the side-attached Majorana state on \downarrow electrons has no analogy to any normal systems [42, 48, 54].

Upon increasing the coupling t_m we observe a gradual splitting of the Andreev quasiparticles, leading to emergence of the effective 'molecular' structure. We can notice some differences appearing in the spectrum $A_\sigma(\omega)$ of \uparrow and \downarrow electrons, especially in the low energy region.

B. Quasiparticle features in tunneling spectroscopy

Low energy quasiparticles of the QD, which is side-attached to the Majorana mode, can be probed in our setup (Fig. 1) only indirectly, via the tunneling current. When voltage V applied between the normal tip and superconducting substrate is smaller than the energy gap Δ the charge transport is provided at low temperatures solely by the Andreev reflections [59]. For noninteracting systems such transport mechanism can be quantitatively determined from the Landauer-type formula

$$I_A(V) = \frac{e}{h} \int d\omega T_A(\omega) [f(\omega - eV) - f(\omega + eV)], \quad (8)$$

where $f(x) = [1 + \exp(x/k_B T)]^{-1}$ is the Fermi distribution. The energy-dependent transmittance

$$T_A(\omega) = \Gamma_N^2 |\mathcal{G}_{12}(\omega)|^2 + \Gamma_N^2 |\mathcal{G}_{21}(\omega)|^2 \quad (9)$$

describes a probability of electron (from STM tip) with spin σ to be converted into a hole (reflected back to the STM tip) with an opposite spin $\bar{\sigma}$, injecting one Cooper pair into the superconducting substrate. Similar expression (8) is valid (subject to certain approximations) also for the correlated quantum dots [60]. It has been emphasized [58], that the differential conductance $G_A(V) = dI_A(V)/dV$ can detect the subgap quasiparticle states, at expense of mixing the particle and hole degrees of freedom. In particular, at zero temperature the differential conductance simplifies to $G_A(V) = \frac{2e^2}{h} [T_A(\omega = +eV) + T_A(\omega = -eV)]$.

Figure 3 shows the differential Andreev conductance obtained at zero temperature for different values of t_m , assuming $\epsilon_m = 0$. We observe, that for all finite couplings $t_m \neq 0$ the linear conductance $G_A(V = 0)$ drops to the value $\frac{1}{4}G_A(V = 0)|_{t_m=0}$. This result is qualitatively different from what has been obtained for N-QD-N junctions, where $G(V = 0)|_{t_m \neq 0} = \frac{3}{4}G(V = 0)|_{t_m=0}$ [42]. Upon increasing the coupling t_m the nonlinear conductance $G_A(V \neq 0)$ develops four local maxima, two of them at $\pm\sqrt{\epsilon^2 + (\Gamma_S/2)^2}$ and additional pair at $\pm\sqrt{\epsilon^2 + (\Gamma_S/2)^2 + (2t_m)^2}$. These local maxima are no longer equal to the perfect Andreev conductance $4e^2/h$.

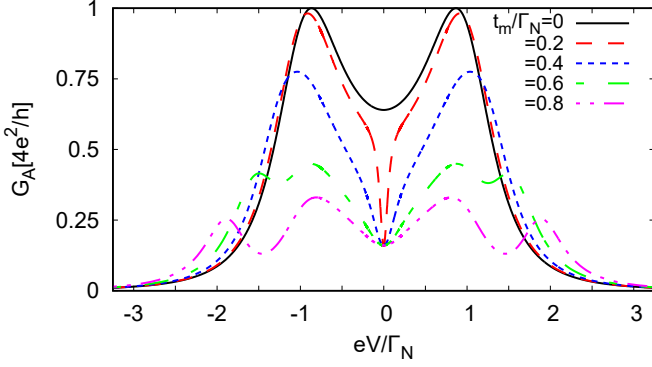


FIG. 3. The differential Andreev conductance obtained at zero temperature for the same model parameters as in Fig. 2.

They originate from the Andreev states mixed with the Majorana quasiparticle (see Fig. 2).

In N-QD-N junctions with the side-attached Majorana nanowire the weak coupling t_m leads to the Fano-type interference patterns [61]. Unlike the usual π shift one obtains in that case only a fraction of such phase. In consequence the density of states is reduced by half and the corresponding linear conductance drops to $3/4$ of its original value, namely to $e^2/h + \frac{1}{2}e^2/h$ as compared to the maximum $2e^2/h$ for $t_m = 0$ case. In our N-QD-S setup (Fig. 1) both spins participate in forming the local pairs. The Andreev current depends on the squared anomalous Green's functions $\mathcal{G}_{12}(\omega)$ and $\mathcal{G}_{21}(\omega)$ therefore the linear conductance $G_A(V = 0)$ is strongly reduced (down to 25%) for arbitrary coupling $t_m \neq 0$ (Fig. 3).

IV. MAJORANA VS KONDO

We now analyze the correlated quantum dot, focusing on the subgap Kondo effect originating from the Coulomb potential U and the coupling Γ_N to the normal STM tip. It has been emphasized [56, 57], that (in absence of the Majorana quasiparticle) the induced on-dot pairing has unique relationship with the Coulomb repulsion. For instance, by increasing the ratio Γ_S/U the subgap Kondo peak would broaden [37, 38] and this behavior shall occur upon approaching the quantum phase transition from the (spinfull) doublet side [55].

Our main purpose here is to examine how this subgap Kondo effect (appearing at zero energy) gets along with the leaking Majorana mode. Some earlier studies of the correlated quantum dot coupled to both normal (conducting) electrodes in presence of the side-attached Rashba chain indicated a competition between the Kondo and Majorana physics [42, 48, 49, 54, 62, 63]. For sufficiently long wire ($\epsilon_m = 0$) the Kondo effect is preserved only for the spin-channel \downarrow (which is not coupled to the Majorana zero-energy mode), whereas for the other spin-channel \uparrow there appears a dip in the spectral density at $\omega = 0$ (reminiscent to what we observed in the upper

panel of Fig. 2). In consequence, the total transmission is partly blocked suppressing the linear conductance from $2e^2/h$ to the fractional value $3e^2/2h$ [41, 42, 48, 49, 54]. For the short Rashba wires ($\epsilon_m \neq 0$) the Kondo physics may survive in both spin channels, with its width dependent on ϵ_m . The initial Kondo features are fully recovered in both of the spin-channels only when $\epsilon_m \gg (|\epsilon|, U, \Gamma)$.

When the correlated quantum dot is embedded between the metallic and superconducting leads (N-QD-S) the eventual subgap Kondo effect is controlled by U/Γ_S ratio and ϵ [37, 38, 56, 58, 64], which decide whether QD ground-state is the (spinfull) doublet $|\sigma\rangle$ or the (spinless) BCS-type $u|0\rangle - v|\uparrow\downarrow\rangle$ configuration. In particular, for the half-filled QD ($\epsilon = -\frac{U}{2}$) the BCS singlet is realized for $U < \Gamma_S$, whereas the doublet is preferred for $U > \Gamma_S$ [55]. Obviously, the Kondo physics might occur only for the latter one, owing to antiferromagnetic exchange interactions driven between the QD and normal lead [38, 65]. In what follows, we confront this subgap Kondo effect with the leaking Majorana quasiparticle.

A. Perturbative treatment of correlations

To study the correlation effects we start by treating the Coulomb term $Un_\downarrow n_\uparrow$ in a perturbative manner. We compute the self-energy matrix $\Sigma(\omega)$ of the single particle Green's function from the Dyson equation $\mathcal{G}^{-1}(\omega) = [\mathcal{G}^{U=0}(\omega)]^{-1} - \Sigma(\omega)$ within the second-order perturbation theory (SOPT) [66], which yields the following diagonal and off-diagonal selfenergies [38, 56]

$$\Sigma_{11}(\omega) = U\langle d_\downarrow^\dagger d_\downarrow \rangle + U^2 \int_{-\infty}^{\infty} \frac{(-\frac{1}{\pi}) \text{Im}\Sigma_{11}^{(2)}(\omega')}{\omega - \omega' + i0^+} d\omega', \quad (10)$$

$$\Sigma_{22}(\omega) = U\langle d_\uparrow^\dagger d_\uparrow \rangle + U^2 \int_{-\infty}^{\infty} \frac{(-\frac{1}{\pi}) \text{Im}\Sigma_{22}^{(2)}(\omega')}{\omega - \omega' + i0^+} d\omega', \quad (11)$$

$$\Sigma_{12}(\omega) = U\langle d_\downarrow d_\uparrow \rangle - U^2 \int_{-\infty}^{\infty} \frac{(-\frac{1}{\pi}) \text{Im}\Sigma_{12}^{(2)}(\omega')}{\omega - \omega' + i0^+} d\omega'. \quad (12)$$

The imaginary parts of the second-order contributions $\Sigma_{ij}^{(2)}(\omega)$ are expressed by the convolutions [65]

$$-\frac{1}{\pi}\text{Im}\Sigma_{11(22)}^{(2)}(\omega) = \int_{-\infty}^{\infty} \left[\Pi_1(\omega + \omega')\rho_{22(11)}^+(\omega') + \Pi_2(\omega + \omega')\rho_{22(11)}^-(\omega') \right] d\omega', \quad (13)$$

$$-\frac{1}{\pi}\text{Im}\Sigma_{12}^{(2)}(\omega) = \int_{-\infty}^{\infty} \left[\Pi_1(\omega + \omega')\rho_{21}^+(\omega') + \Pi_2(\omega + \omega')\rho_{21}^-(\omega') \right] d\omega', \quad (14)$$

where

$$\Pi_{1(2)}(\omega) = \int_{-\infty}^{\infty} \left[\rho_{11}^{-(+)}(\omega')\rho_{22}^{-(+)}(\omega - \omega') - \rho_{12}^{-(+)}(\omega')\rho_{21}^{-(+)}(\omega - \omega') \right] d\omega', \quad (15)$$

and $\rho_{ij}^{\pm}(\omega) \equiv \frac{-1}{\pi}\text{Im}\mathcal{G}_{ij}^0(\omega + i0^+)f(\pm\omega)$ denote the occupancies obtained from the uncorrelated Green's functions (4), taking into account the effective dot level and influence of the superconducting electrode [56].

Let us inspect the spectral function of the correlated quantum dot for each spin separately. Figure 4 shows the results obtained at zero temperature by perturbative treatment of the Coulomb potential. The top panel refers to N-QD-S junction in absence of the Majorana mode. In the weak interaction U regime it is characterized by two Andreev peaks. When approaching $U \approx \Gamma_S$ these quasiparticle peaks merge, signaling the quantum phase transition (formally for $\Gamma_N \neq 0$ it becomes a continuous crossover). In the strongly correlated limit ($U > \Gamma_S$), we observe development of the subgap Kondo peak at $\omega = 0$ whose broadening gradually shrinks upon increasing the ratio U/Γ_S which has been explained in Refs [38, 56].

In the presence of the side-attached nanowire we notice, that the Majorana mode has completely different influence on each spin channel (panels b and c in Fig. 4). In some analogy to the non-interacting case the spectral function $A_{\uparrow}(\omega)$ reveals a depletion of the electronic states near $\omega \sim 0$. We assign it to destructive interference caused by the side-attached Majorana mode [35]. The other spectral function $A_{\downarrow}(\omega)$ shows an opposite effect. Indirect coupling of spin \downarrow electrons with the Majorana mode contributes more states near zero energy, the Kondo peak seems thus to be magnified.

The subgap QD spectrum can be probed by the Andreev scattering which would engage both the spin components, we hence display (Fig. 5) evolution of the total spectral function $A(\omega) = \sum_{\sigma} A_{\sigma}(\omega)$ for various couplings t_m and Coulomb potential U (as indicated). Already in the weakly correlated limit the initial Kondo peak is substantially suppressed. Upon increasing the Coulomb potential U the QD spectrum develops two separated Andreev quasiparticle states (broadened by Γ_N), coexisting with the Majorana feature. This behavior is

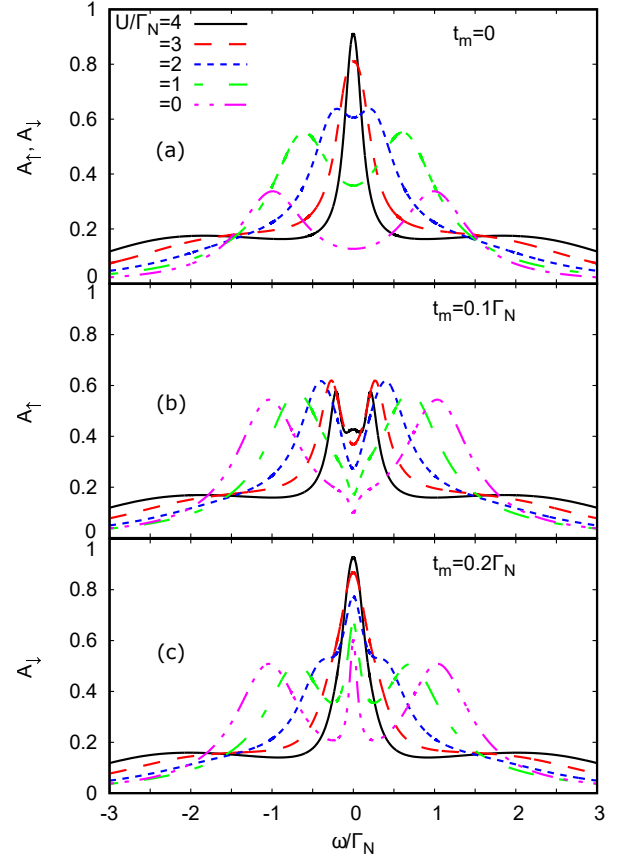


FIG. 4. The spin-resolved spectral function $A_{\sigma}(\omega)$ obtained by the SOPT method at zero temperature for the half-filled quantum dot ($\epsilon = -U/2$), using $t_m = 0$ (upper panel) and $t_m/\Gamma_N = 0.2$ (middle/bottom panels).

reminiscent of the exact solution in the superconducting atomic limit $\Gamma_N = 0$ (see Figs. 16 and 17). On the other hand, for stronger coupling $t_m = 0.8\Gamma_N$ the spectral function acquires qualitatively different ‘molecular’ structure, in which the leaking Majorana mode is strongly mixed with the initial QD quasiparticle states. Under such circumstances we can hardly discriminate signatures of the Kondo state from Majorana quasiparticle.

B. NRG results

For reliable analysis of the correlations, the induced electron pairing and the leaking Majorana quasiparticle, we have also performed calculations, based on the numerical renormalization group (NRG) algorithm [67]. Our purpose was to study the low energy spectrum of the

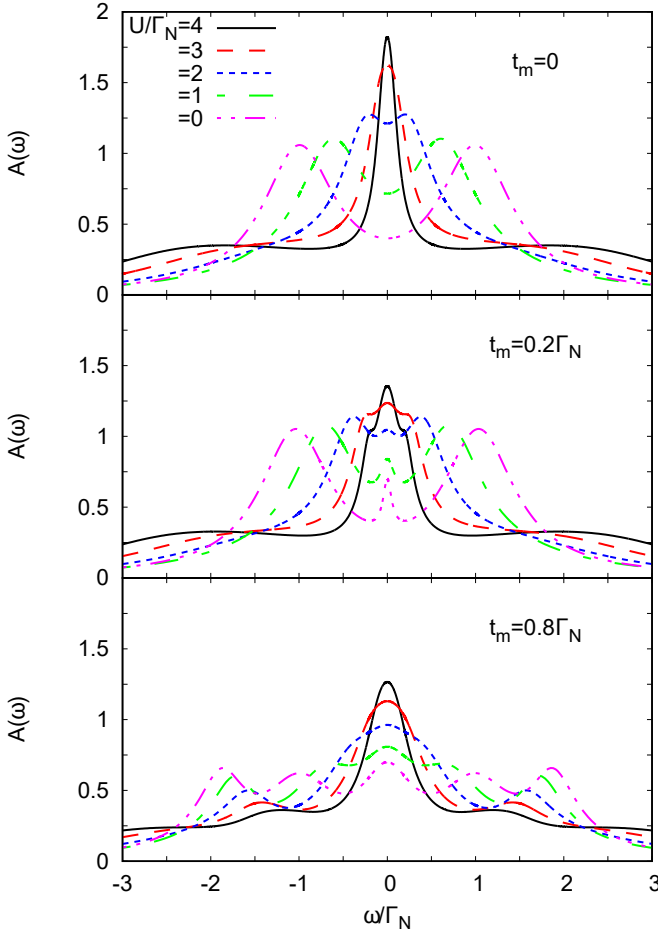


FIG. 5. The total normalized spectral function $A(\omega) = \sum_{\sigma} A_{\sigma}(\omega)$ of the half-filled quantum dot ($\varepsilon = -U/2$) obtained at $T = 0$ for $\Gamma_S = 2\Gamma_N$ and several values of the Coulomb potential U (as indicated), assuming (a) $t_m = 0$, (b) $t_m = 0.2$, and (c) $t_m = 0.8$. All energies are expressed in units of Γ_N .

following effective model

$$\begin{aligned}
 H = & \sum_{\sigma} \epsilon d_{\sigma}^{\dagger} d_{\sigma} + U n_{\downarrow} n_{\uparrow} - \frac{\Gamma_S}{2} (d_{\uparrow} d_{\downarrow} + d_{\downarrow}^{\dagger} d_{\uparrow}^{\dagger}) \\
 & + t_m (d_{\uparrow}^{\dagger} - d_{\uparrow})(f + f^{\dagger}) + \epsilon_m \left(f^{\dagger} f - \frac{1}{2} \right) \\
 & + H_N + H_{N-QD}.
 \end{aligned} \tag{16}$$

This Hamiltonian (16) corresponds to the single-channel model, allowing for a good quality computational analysis. We have performed the NRG calculations using the Budapest Flexible DM-NRG code [68] for constructing the zero-temperature density matrix of the system and calculating the corresponding spin-resolved spectral functions for arbitrary model parameters. Because the coupling to Majorana zero-energy mode and superconducting pairing correlations break the spin and charge symmetries, only the charge parity symmetry of the total Hamiltonian was used. In calculations we kept at least 1024 states per iteration and imposed the discretiza-

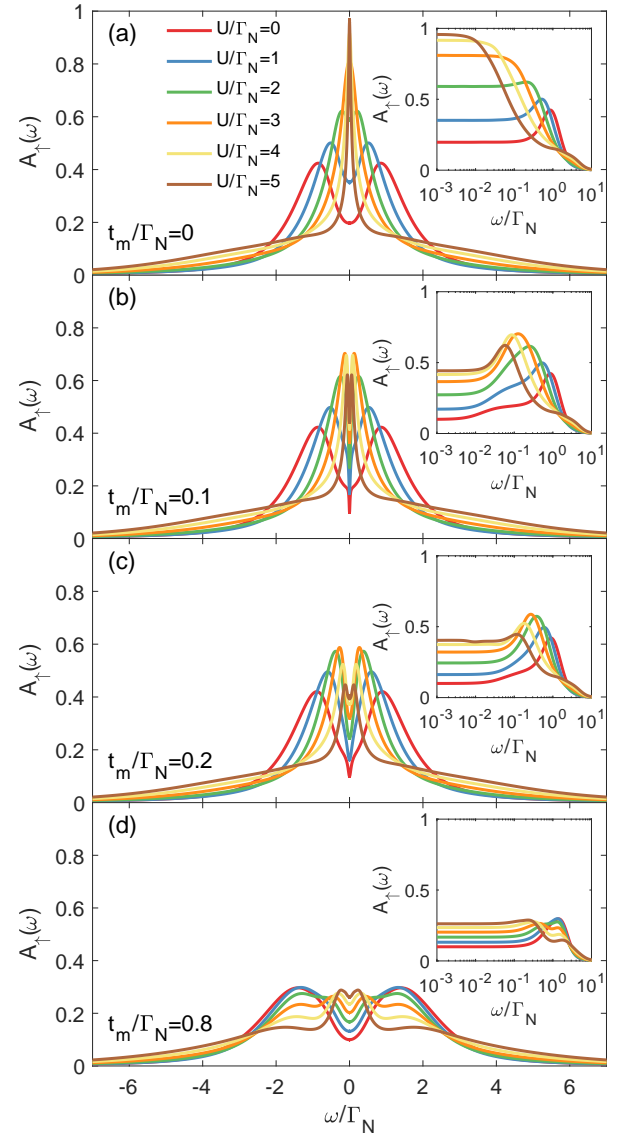


FIG. 6. The normalized spectral function $A_{\uparrow}(\omega)$ for spin \uparrow obtained from NRG calculations for $\Gamma_S = 2\Gamma_N$, various ratios of U/Γ_N (displayed in the legend of the upper panel) and several values of the coupling t_m , as indicated. The other parameters are $\epsilon = -U/2$, $\epsilon_m = 0$ and $\Gamma_N = D/50$, with D the band halfwidth.

tion parameter $\Lambda = 2$. Our results were averaged over $N_z = 4$ interleaved discretizations [69], using the logarithmic Gaussian broadening to obtain the smooth spectral functions. We have assumed the flat density of states of the normal lead with a cutoff $D \gg U$, with D being the band halfwidth.

Figures 6 and 7 present the spectral functions obtained by NRG for spin \uparrow and \downarrow , respectively. Since we are interested in what happens to the Kondo state due to the side-attached Majorana mode, we additionally display the low energy spectrum in the logarithmic scale (in the insets). Quasiparticle states of \uparrow electron (directly coupled to the Majorana mode) are strongly suppressed near $\omega \sim 0$. In

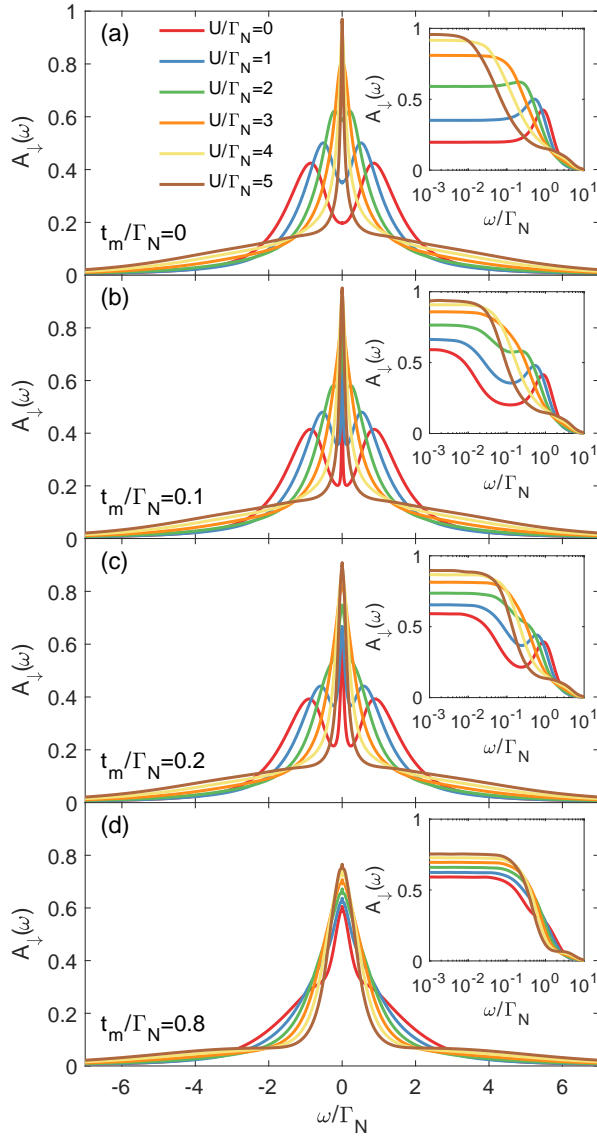


FIG. 7. The spectral function $A_{\downarrow}(\omega)$ obtained by the NRG calculations for the same set of parameters as in Fig. 6.

the weak Majorana-dot coupling regime (b & c panels) we assign such effect to the destructive quantum interference [35]. For stronger coupling $t_m = 0.8\Gamma_N$, the QD states are hybridized with the Majorana mode, reducing the zero-energy spectral function and developing the new (molecular) quasiparticles. This is particularly evident when inspecting the inset of Fig. 6(d).

The spin \downarrow sector (Fig. 7) reveals an opposite tendency. In this case, the Majorana mode indirectly affects the states predominantly in a vicinity of $\omega \sim 0$. In the weak coupling limit the Kondo effect (existing for $U \geq \Gamma_S$) seems to be robust, but its shape slightly broadens (see the insets of panels b & c). In the molecular regime (panel d) the electronic states cumulate near the zero energy, forming a single structureless peak. We interpret it as an indirect leakage of the Majorana quasiparticle

driven by the on-dot pairing.

Our numerical results obtained by the unbiased NRG calculations qualitatively agree with the selfconsistent perturbative treatment. For the Majorana mode weakly coupled to the QD, both methods show its detrimental influence on the subgap Kondo effect of \uparrow spin and less severe (almost neutral) effect on \downarrow spin sector. In the latter case the Kondo peak seems to be robust (it merely broadens). On the other hand, for the QD strongly coupled to the nanowire we find influence of the leaking Majorana mode on both spin sectors, where it redistributes the overall quasiparticle spectra. Under such circumstances the Kondo state is no longer evident.

C. Andreev conductance

Verification of the above mentioned effects could be possible by measuring the Andreev current, cf. (8). Fig-

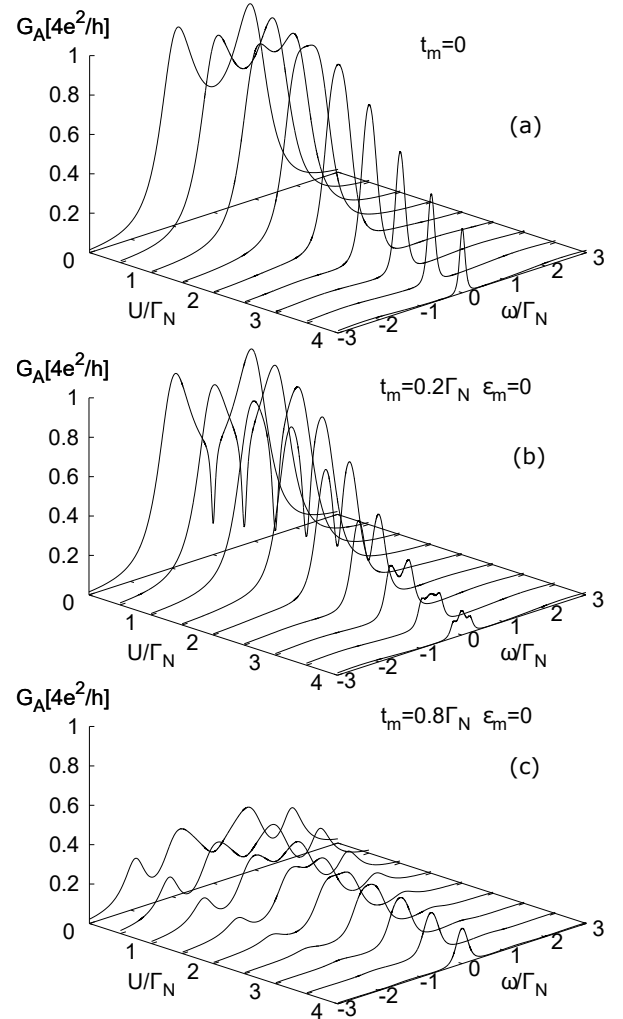


FIG. 8. The differential subgap conductance $G_A(V)$ as a function of the applied voltage V and the Coulomb potential U obtained at $T = 0$ for the half-filled QD, using $\Gamma_S = 2\Gamma_N$.

ure 8 shows the variation of the differential Andreev conductance $G_A(V)$ with respect to the Coulomb potential U for the weak (b) and strong (c) coupling t_m limits, respectively. Due to technical limitations (related with numerical precision for computation of the real part of the anomalous Green's function) we show here the results obtained within the perturbative scheme. In the weakly correlated case these plots resemble the results presented in Fig. 3 for the uncorrelated QD. Qualitative changes appear at stronger U , especially on the doublet side $U \geq \Gamma_S$.

In the absence of the Majorana mode ($t_m = 0$) the differential conductance is characterized by two peaks at bias V , coinciding with energies of the Andreev states. The additional zero-bias enhancement is due to the subgap Kondo effect, appearing in the doublet region (i.e. for $U \geq \Gamma_S$). Within the generalized Schrieffer-Wolff approach adopted for the N-QD-S setup we have previously estimated [38], that the effective Kondo temperature of half-filled QD scales as $\ln T_K \propto 1/\left[1 - \left(\frac{\Gamma_S}{U}\right)^2\right]$. In particular, it yields enhancement of T_K with respect to Γ_S upon approaching the doublet-singlet transition. This unique behavior is valid for arbitrary Δ , as has been found by the NRG studies [37]. In the limit of $U \gg \Gamma_S$, the Andreev tunneling is strongly suppressed, because the off-diagonal Green's function (characterizing efficiency of the induced on-dot pairing) rapidly diminishes. We illustrate these effects in the upper panel of Fig. 8.

Leakage of the Majorana mode on the QD remarkably affects the mentioned behavior. In the weak coupling limit (middle panel of Fig. 8) its influence merely shows up near the zero-bias conductance. For $\Gamma_S \sim U$, we observe a superposition of the leaking Majorana feature (whose width depends on t_m) with leftovers of the Kondo peak, surviving in spin \downarrow channel. For the strong coupling t_m (bottom panel of Fig. 8), the differential conductance $G_A(V)$ develops the 'molecular' structure, characterized by four peaks. We interpret them as the bonding and anti-bonding mutations of the initial Andreev quasiparticles caused by hybridization with the Majorana mode.

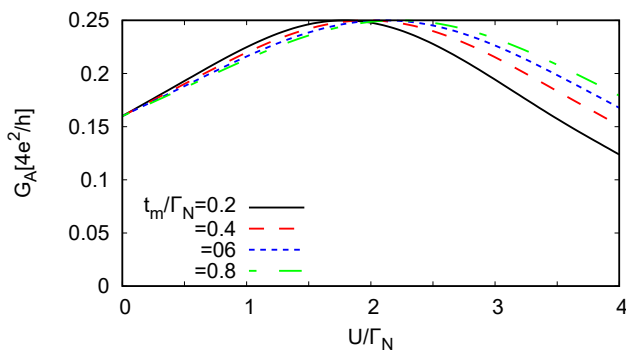


FIG. 9. The zero-bias Andreev conductance $G_A(V=0)$ versus the Coulomb potential U (in units of Γ_N) obtained perturbatively for $\epsilon = -U/2$, $\Gamma_S = 2\Gamma_N$, $\epsilon_m = 0$.

rana mode. Upon increasing the Coulomb potential the internal peaks gradually merge into a single central one, whereas the external peaks lose their spectral weights.

We notice some universal feature, originating from the Majorana mode in the linear conductance with respect to the Coulomb potential (Fig. 9). Its optimal value e^2/h is 4 times smaller than the one obtained for the N-QD-S system without the side-attached Majorana mode [64, 70]. Maximum of the zero bias conductance $G_A(V=0)$ occurs at $U \approx \Gamma_S$, which corresponds to a crossover between the spinless and spinfull configurations [64]. For $t_m \neq 0$, this maximum slightly shifts towards $U > \Gamma_S$, suggesting that the leaking Majorana mode does affect (though weakly) the singlet-doublet phase transition.

V. SUMMARY AND DISCUSSION

We have analyzed the spin-resolved spectroscopic features of the quantum dot side-coupled to the topologically superconducting nanowire, hosting the Majorana quasiparticles. Focusing on an STM-type geometry we have investigated its subgap electronic spectrum which can be probed by the Andreev tunneling, that simultaneously involves the particle and hole degrees of freedom.

In the uncorrelated case ($U = 0$) the presence of the Majorana quasiparticle induces either the zero-energy peak or dip in the QD spectral density, depending on the spin (Fig. 2). These effects originate from the constructive or destructive quantum interference [61]. Our study predicts, that the differential Andreev conductance would be predominantly affected by a destructive interference, leading to the zero-bias dip preserved from the weak to strong hybridization t_m regimes.

We have also inspected the correlated quantum dot ($U \neq 0$) case, addressing interplay between the on-dot pairing with the Kondo effect in the presence of the leaking Majorana quasiparticle. The Coulomb interaction along with the proximity induced electron pairing lead to the quantum phase transition from the spinless to spinfull configurations [55, 57]. When QD is additionally coupled to the normal electrode ($\Gamma_N \neq 0$) such transition changes into a crossover and simultaneously the effective spin exchange (between QD and itinerant electrons) can induce the subgap Kondo effect [37, 38]. By the self-consistent treatment of the Coulomb potential U and using the unbiased NRG calculations we have found that the side-attached Majorana mode would have spin-selective influence of this subgap Kondo effect. For spin \uparrow (directly coupled to the Majorana mode) it would be detrimental, whereas for spin \downarrow we predict an opposite tendency.

This spin-dependent influence of the Majorana mode on the subgap Kondo effect shows up in the low-energy spectrum of the QD. Such property can be added to the previously reported examples of: spin-selective Andreev processes [71], spin-resolved current correlations [72], or non-local spin blocking effect [73], which are unique consequences of the Majorana quasiparticles. Signatures of

the spin-selective influence on the Kondo effect might be, however, difficult to detect in the Andreev tunneling because both spins are mixed (via particle-hole degrees of freedom). Nevertheless, we predict some universal features. For instance, the linear conductance shall be reduced to 25 % of its perfect value typical for N-QD-S junctions [57]. This is in contrast to what has been predicted for N-QD-N junctions, where the single particle conductance is reduced only to 75 % of the unitary value [42]. Yet in both cases the underlying mechanism is related to the very same fractional character of the Majorana quasiparticles.

Our study of the Kondo state vs Majorana mode relationship is different from the previous considerations of the topological Kondo effect that could be realized in the correlated nanowires [62, 63, 74–77]. We hope that this analysis of the proximized quantum dot hybridized with the Majorana nanowire (Fig. 1) would be experimentally feasible in STM measurements and could verify nontrivial interplay between the on-dot pairing, the Kondo effect, and the exotic Majorana quasiparticles.

ACKNOWLEDGMENTS

This work is supported by the National Science Centre in Poland via projects Nos. DEC-2014/13/B/ST3/04451 (TD) and DEC-2013/10/E/ST3/00213 (IW), and the Faculty of Mathematics and Natural Sciences of the University of Rzeszów through the Project No. WMP/GD-06/2017 (GG).

Appendix A: Short wire case

Main part of this paper is devoted to the infinitely long nanowire, where the Majorana modes do not overlap ($\epsilon_m = 0$) with each other. The Kondo state and the Majorana quasiparticle are there manifested at $\omega = 0$. In finite nanowires the Majorana modes partly overlap ($\epsilon_m \neq 0$). For $\Gamma_N = 0$ and $U = 0$ we obtain six quasiparticle states: two Andreev bound states ($\omega_{\pm} \pm \sqrt{\epsilon^2 + (\Gamma_S/2)^2}$) and four other ones mixed with the Majorana modes $\omega_{\pm} \pm (X/2 \pm 1/2 \sqrt{X^2 - 4\epsilon_m^2(\epsilon^2 + \Gamma_S^2/4)})^{0.5}$, where $X = \epsilon^2 + \epsilon_m^2 + \Gamma_S^2/4 + 4t_m^2$. For $U \neq 0$ and $\Gamma_N \neq 0$ these quasiparticle states appear away from the Fermi energy, so they are less influential on the Kondo effect. Figure 10 presents the total spectral function obtained for two values of ϵ_m in the Kondo regime. For small $\epsilon_m = 0.2\Gamma_N$ (Fig. 10a) and in the weak interaction limit, we observe six subgap quasiparticle peaks. With increasing U , two of them merge into the Kondo resonance peak (for $U \geq \Gamma_S$) with a tiny superstructure at $\omega = 0$. For large overlap $\epsilon_m = 1.5\Gamma_N$ (Fig. 10b), we obtain the spectrum reminiscent of the N-QD-S system (Fig. 5a) with only a redistribution of the spectral weight at higher energies.

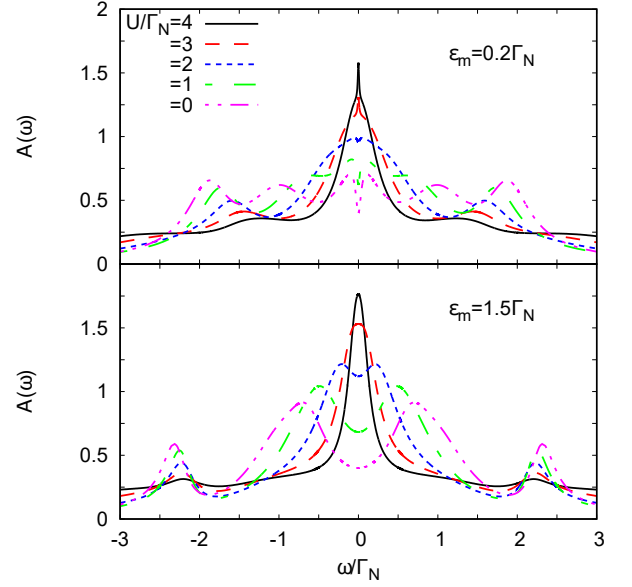


FIG. 10. The total spectral function $A(\omega)$ of the correlated dot obtained for different values of U , using $\Gamma_S = 2\Gamma_N$, $\epsilon = -U/2$, $t_m = 0.8\Gamma_N$, $\epsilon_m = 0.2\Gamma_N$ (a) and $\epsilon_m = 1.5\Gamma_N$ (b).

Finite overlap ϵ_m would show in the differential Andreev conductance. Figure 11 shows $G_A(V)$ as a function of the applied voltage V for the weakly ($\epsilon_m = 0.2\Gamma_N$) and strongly ($\epsilon_m = 1.5\Gamma_N$) overlapping Majorana modes. In the first case we observe the well pronounced zero-bias peak of a narrow width, dependent on ϵ_m . Optimal

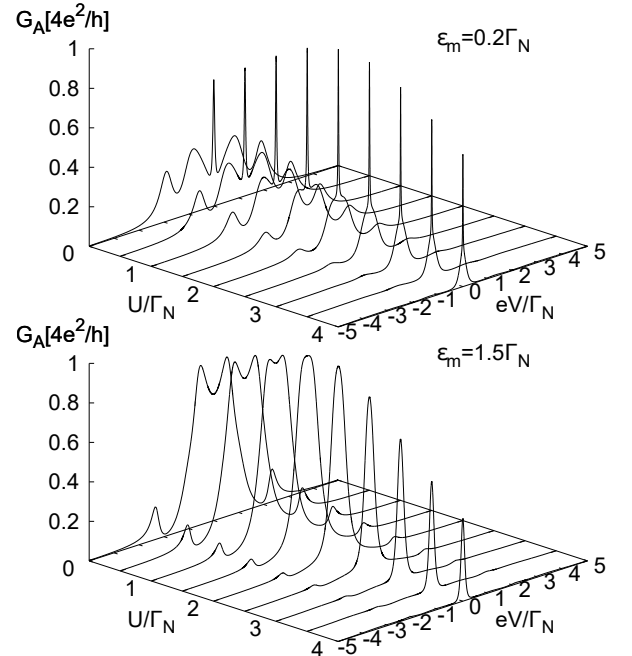


FIG. 11. The differential Andreev conductance G_A as a function of the applied voltage eV for $\Gamma_S = 2\Gamma_N$, $\epsilon = -U/2$, $\epsilon_m = 0.2\Gamma_N$ (a) and $\epsilon_m = 1.5\Gamma_N$ (b).

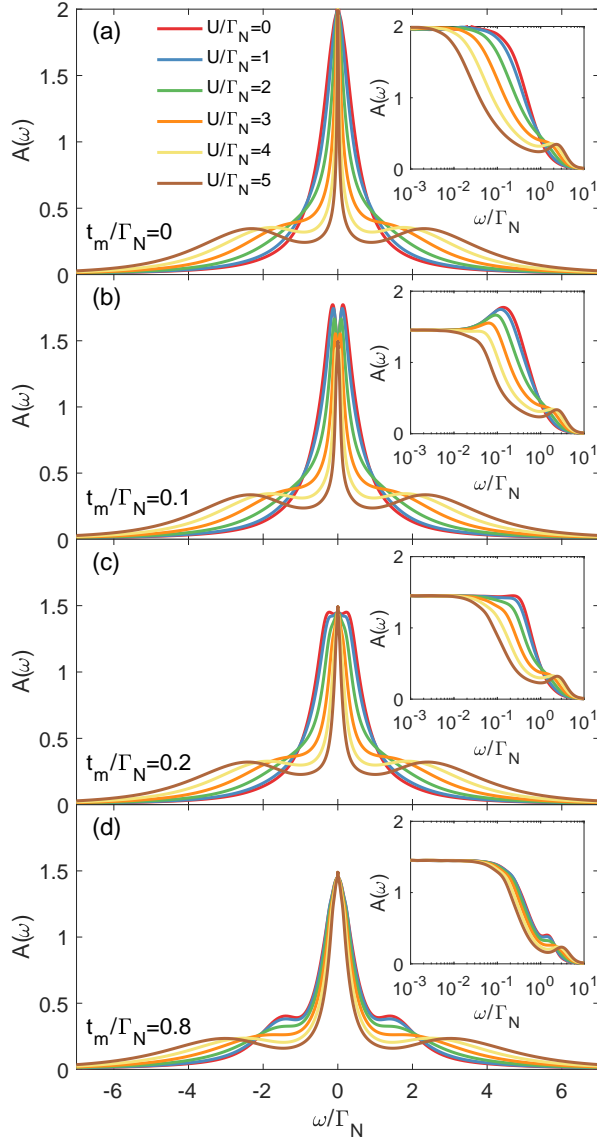


FIG. 12. The total spectral function of the half-filled quantum dot coupled only to the normal lead ($\Gamma_S = 0$). Results are obtained by NRG for various Coulomb potentials (indicated in the legend) and several couplings to the Majorana mode $t_m/\Gamma_N = 0, 0.1, 0.2$, and 0.8 , assuming $\epsilon_M = 0$. The other parameters are the same as in Fig. 6.

value of the zero-bias peak approaches $4e^2/h$ for $U \approx \Gamma_S$. For $U < \Gamma_S$, we observe two Andreev and two other Majorana-Andreev hybrids, appearing in the differential conductance. With increasing U , the Andreev peaks evolve into the central peak, appearing at $V = 0$. On the other hand, for the short nanowire ($\epsilon_m = 1.5\Gamma_N$) and at small voltages, the differential conductance $G_A(eV)$ is similar as for N-QD-S system [38].

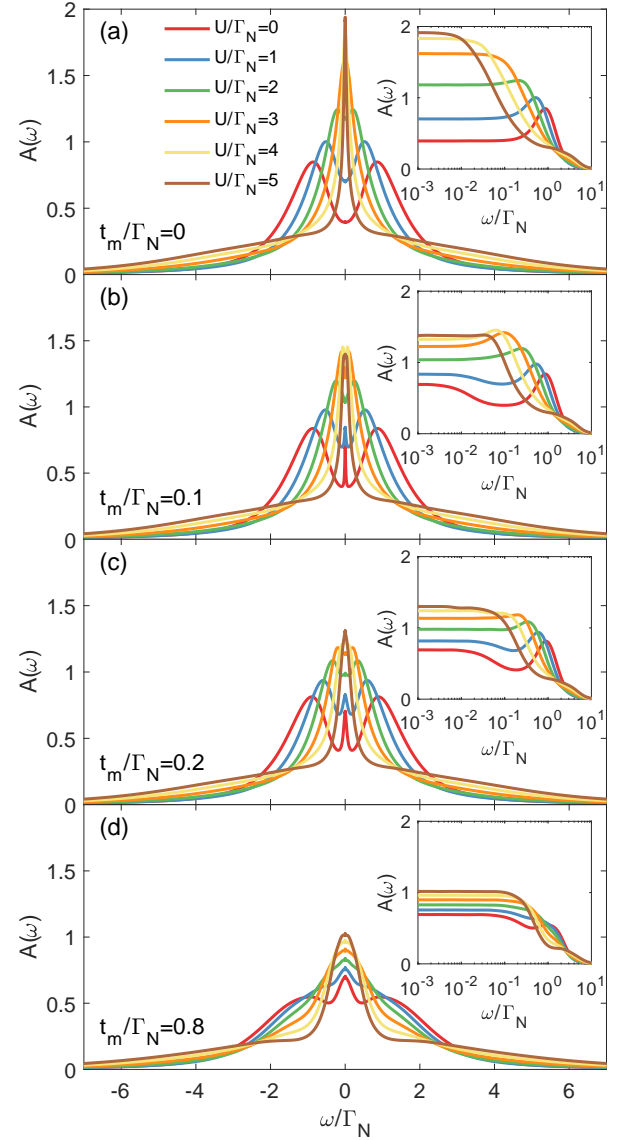


FIG. 13. The same as in figure 12, but for $\Gamma_S = 2\Gamma_N$.

Appendix B: Comparison with the normal QD

It might be instructive to give a comparison of the correlated quantum dot spectrum (discussed in Sec. IV) with the one, when on-dot pairing is absent. We present here such results for the half-filled QD obtained by the nonperturbative NRG calculations.

Figure 12 displays the total spectrum of the ‘normal’ QD, corresponding to the situation $\Gamma_S = 0$. For $t_m = 0$, we recognize the widely known structure with two quasi-particle peaks at ϵ and $\epsilon + U$ and the Kondo peak at the Fermi level (whose broadening depends on U and Γ_N). The side-attached Majorana mode leads to noticeable changes mainly near the Fermi level, by suppressing the Kondo peak for the spin \uparrow electrons, whereas the other spin is completely unaffected by the Majorana. For strong couplings t_m we observe development of the

‘molecular’ structure, in which the quasiparticle states are no longer present at ϵ and $\epsilon + U$.

This can be contrasted with our N-QD-S setup, taking into account the proximity induced on-dot pairing $\Gamma_S \neq 0$. For each spin sector we have discussed already the corresponding spectra in Sec. IV B. Let us briefly comment on the total spectral function presented in Fig. 13. For $t_m = 0$ (top panel in Fig. 13), we recognize the spinless to spinfull quantum phase transition/crossover at $\Gamma_S \sim U$ discussed previously in Refs [37, 38], where the Kondo effect is observable on the spinfull side (i.e. for $\Gamma_S \leq U$). Leakage of the Majorana mode (for $t_m \neq 0$) suppresses this subgap Kondo peak, as can be clearly visible in the logarithmic scale (see the insets). On the other hand, on the BCS-type side (corresponding to $\Gamma_S > U$) we practically see the separated Andreev peaks coexisting with a tiny feature at $\omega = 0$ due to the leaking Majorana mode. Such comparison of Figs 12 and 13 emphasizes a qualitative influence of the proximity-induced pairing on the Kondo-Majorana interplay.

Appendix C: Influence of magnetic field

In realistic situations the Majorana end-modes emerge in the proximized nanowire only above some critical magnetic field on the order of 1 Tesla [23]. The external magnetic field can have strong influence on the quantum dot (coupled to the Majorana modes) and on the resulting transport properties. Let us recall, that in experimental setup of the Copenhagen group [29, 78] the finite-energy (Andreev) and the zero-energy (Majorana) quasiparticle states leak from the nanowire to the ‘normal’ quantum dot. Actually, upon increasing the magnetic field there has been observed a coalescence of one pair of the Andreev bound states into the zero-energy Majorana mode. The quantum dot played a role of the spectrometer.

Here we consider a different N-QD-SC setup, in which the quantum dot develops its initial Andreev states owing to the proximity with the superconducting substrate. The side-attached nanowire contributes the Majorana mode, which modifies the QD spectrum. Obviously, the magnetic field would strongly affect the subgap spectrum of such ‘proximitized’ QD. Within our model described by the low-energy Hamiltonian (1,2) we can consider the magnetic field through the spin-dependent energy levels $\epsilon_\downarrow = \epsilon + V_Z$ and $\epsilon_\uparrow = \epsilon - V_Z$ with the Zeeman splitting $2V_Z = g\mu_B B$ [31, 79, 80].

To present this influence of magnetic field we focus on the strongly asymmetric coupling $\Gamma_S = 4\Gamma_N$, when the bound states are well pronounced (their broadening is then rather narrow). For brevity we show in Fig. 14 the differential Andreev conductance as a function of Zeeman splitting energy V_Z obtained for a moderate coupling $t_m = 0.4\Gamma_N$ with Majorana mode. For the uncorrelated quantum dot (see the upper panel), we observe at $V_Z = 0$ two maxima (corresponding to the Andreev states energies) where the conductance is $G_A = 4e^2/h$.

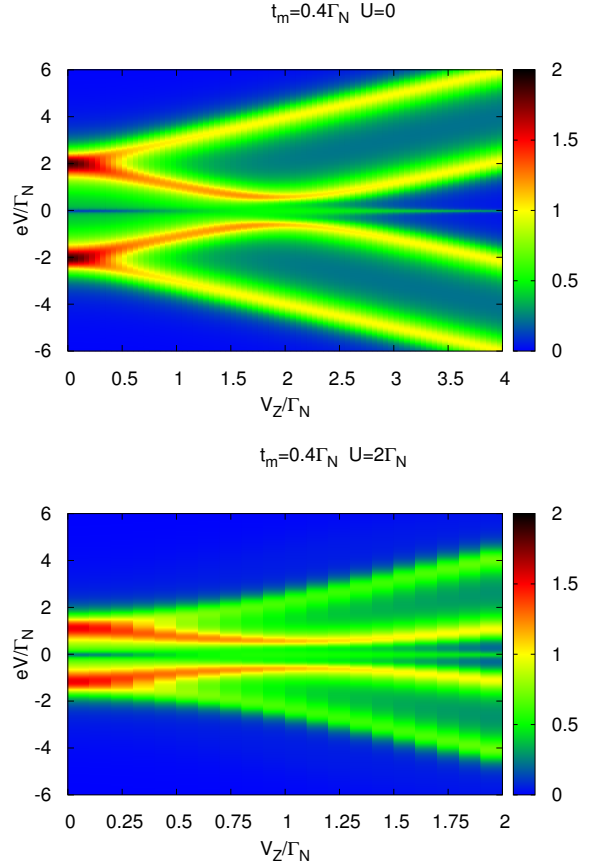


FIG. 14. The differential Andreev conductance $G_A(V)$ [in units of $\frac{2e^2}{h}$] as function of voltage V and Zeeman splitting V_Z obtained at zero temperature, using $\Gamma_S = 4\Gamma_N$, $U = 0$ (top panel) and $U = 2\Gamma_N$ (bottom panel).

Upon increasing the magnetic field they split and the internal branches start to approach, but they never cross each other. At some critical magnetic field the internal branches are pushed aside, and simultaneously there emerges the zero-bias conductance peak (ZBCP) signaling the leaking Majorana mode. Similar tendency (for the ‘normal’ quantum dots) has been reported recently by several groups [78, 81]. We have checked that in our setup this ZBCP achieves the optimal value near $V_Z \approx \Gamma_S/2$ and for stronger magnetic fields this zero-bias conductance partly diminishes.

For the correlated case (bottom panel), the optimal differential conductance (which is $G_A < 4e^2/h$) occurs at the renormalized Andreev energies. Again, the magnetic field has quite similar influence on $G_A(V)$. The emerging ZBCP shows at $2V_Z + U \approx \Gamma_S$. We thus conclude that, in our N-QD-SC system with the side-attached Majorana wire, the ZBCP can be induced above some critical magnetic field and its value depends on the Coulomb potential U . Such appearance of the Majorana quasiparticles from the coalescing Andreev states is more exotic than in ‘normal’ quantum dots coupled to the Majorana modes.

Influence of the magnetic field on the subgap Kondo effect shall be discussed elsewhere, because there are a few characteristic energy-scales controlling this effect.

Appendix D: Majorana coupled to both spins

In realistic situations the spin-orbit coupling along with the Zeeman effect break a spin-rotational symmetry of the system. Formally, spin is hence no longer a good quantum number. Physically it means, that such nanowire with the strong spin-orbit interactions brought in contact with superconductor develops the intersite pairing of equal but ‘tilted’ spins. Nevertheless one can project such pairing onto \uparrow and \downarrow components. In each of these sectors the intersite-pairing is characterized by different amplitudes, depending mainly on the magnetic

field. In practice, the Majorana quasiparticles appear simultaneously in both spin channels, but with different spectral weights. This polarization of the Majorana modes has been recently considered by one of us [82] and its experimental evidence has been indeed reported by A. Yazdani and coworkers from STM measurements of *Fe* atoms nanochain using the ferromagnetic tip [28].

Since magnetic polarization of the Majorana modes is in fact relevant, we have considered the coupling of both QD spins to Majorana modes

$$H_{MQD} = t_{m\uparrow}(d_{\uparrow}^{\dagger} - d_{\uparrow})(f + f^{\dagger}) + t_{m\downarrow}(d_{\downarrow}^{\dagger} - d_{\downarrow})(f + f^{\dagger}) + \epsilon_m f^{\dagger} f + \frac{\epsilon_m}{2}. \quad (D1)$$

For the uncorrelated quantum dot the Green’s function takes the following form

$$\mathcal{G}^{-1}(\omega) = \begin{pmatrix} \omega - \epsilon_{\uparrow} + i\Gamma_N/2 & 0 & 0 & \Gamma_S/2 & -t_{m\uparrow} & -t_{m\uparrow} \\ 0 & \omega + \epsilon_{\uparrow} + i\Gamma_N/2 & -\Gamma_S/2 & 0 & t_{m\uparrow} & t_{m\uparrow} \\ 0 & -\Gamma_S/2 & \omega - \epsilon_{\downarrow} + i\Gamma_N/2 & 0 & -t_{m\downarrow} & -t_{m\downarrow} \\ \Gamma_S/2 & 0 & 0 & \omega + \epsilon_{\downarrow} + i\Gamma_N/2 & t_{m\downarrow} & t_{m\downarrow} \\ -t_{m\uparrow} & t_{m\uparrow} & -t_{m\downarrow} & t_{m\downarrow} & \omega - \epsilon_m & 0 \\ -t_{m\uparrow} & t_{m\uparrow} & -t_{m\downarrow} & t_{m\downarrow} & 0 & \omega + \epsilon_m \end{pmatrix}, \quad (D2)$$

For specific calculations, we have assumed imposed

$$\begin{aligned} t_{m\uparrow} &= t_m p \\ t_{m\downarrow} &= t_m (1 - p) \end{aligned}$$

where p accounts for the asymmetric coupling of each spin component. Fig. 15 shows the bias voltage dependence of the Andreev conductance $G_A(eV)$ obtained at zero temperature for several values of parameter p , as indicated. The differential conductance is even with respect to $V = 0$, so we present in the left h.s. panel results for $p < 0.5$ and in the right h.s. panel for $p > 0.5$,

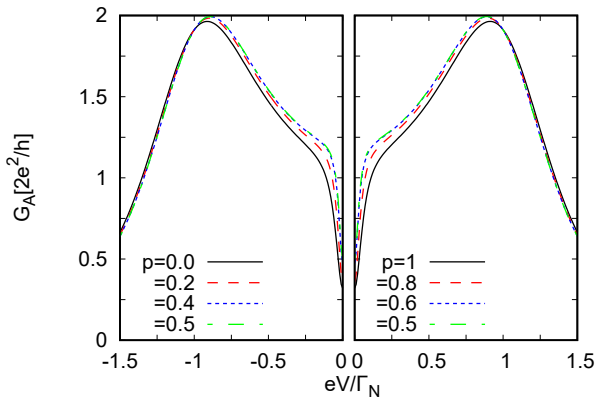


FIG. 15. The differential Andreev conductance $G_A(V)$ [in units of $\frac{2e^2}{h}$] as function of voltage V obtained for the half-filled uncorrelated QD at zero temperature, using $\Gamma_S = 2\Gamma_N$.

respectively. We notice that assymetry has rather negligible influence on the Andreev conductance (it slightly affects only a width of the Majorana interferometric feature). This can be assigned to the fact that Andreev processes equally involve both spins, therefore $G_A(eV)$ symmetrizes the contributions of each sector. We thus conclude, that in our setup (Fig. 1) some influence of a polarized coupling to the Majorana modes would be rather residual. More detailed analysis of this problem (considering the correlations) is beyond a scope of this paper, therefore we shall discuss it elsewhere.

Appendix E: Superconducting atomic limit

To gain some insight into the singlet-doublet quantum phase transition (discussed in main part of this paper), let us first consider the limit $\Gamma_S \gg \Gamma_N$, assuming $\Gamma_N = 0^+$. Influence of the Coulomb repulsion U on the subgap Andreev states in such ‘superconducting atomic limit’ has been first addressed by E. Vecino *et al* [66]. In the absence of the Majorana modes the effective bound states of such problem have been discussed in the review paper [83]. For the present setup we consider the effective Hamiltonian

$$\begin{aligned} H_{QD}^{\text{eff}} &\simeq \sum_{\sigma} \epsilon d_{\sigma}^{\dagger} d_{\sigma} + U n_{\downarrow} n_{\uparrow} - \frac{\Gamma_S}{2} (d_{\uparrow} d_{\downarrow} + d_{\downarrow}^{\dagger} d_{\uparrow}^{\dagger}) \\ &+ t_m (d_{\uparrow}^{\dagger} - d_{\uparrow})(f + f^{\dagger}) + \epsilon_m \left(f^{\dagger} f + \frac{1}{2} \right). \end{aligned} \quad (E1)$$

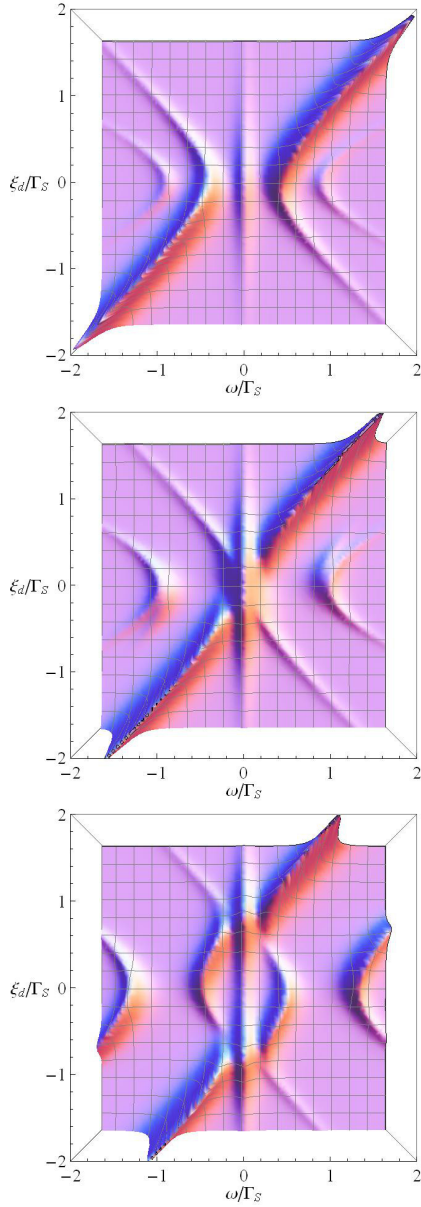


FIG. 16. The spectral function $A_{\uparrow}(\omega)$ of the correlated and proximitized QD obtained in the limit $\Gamma_N \rightarrow 0$, using $t_m/\Gamma_S = 0.3$, $U/\Gamma_S = 0.05$ (top panel), 1 (middle panel), and 2 (bottom panel). Calculations have been done by numerical diagonalization of the Hamiltonian (E1) subject to a small line broadening (that mimics finite life-time).

Following Ref. [55] let us introduce the shorthand notations for the induced on-dot pairing $\Delta_d \equiv \frac{\Gamma_S}{2}$ and for the shifted QD level $\xi_d \equiv \epsilon + \frac{U}{2}$, respectively.

In the absence of the Majorana mode ($t_m = 0$), the true eigenstates are represented by the doublet configurations $|\uparrow\rangle$ and $|\downarrow\rangle$ (corresponding to spin $S = \frac{1}{2}$) and the BCS-like singlet states ($S = 0$)

$$|\Psi_{-}\rangle = u_d |0\rangle - v_d |\uparrow\downarrow\rangle, \quad (\text{E2})$$

$$|\Psi_{+}\rangle = v_d |0\rangle + u_d |\uparrow\downarrow\rangle. \quad (\text{E3})$$

with eigenenergies $E_{\pm} = \xi_d \pm \sqrt{\xi_d^2 + \Delta_d^2}$ and BCS coefficients $u_d^2 = \frac{1}{2} \left[1 + \frac{\xi_d}{E_d} \right] = 1 - v_d^2$, where $E_d = \sqrt{\xi_d^2 + \Delta_d^2}$. In the presence of the side-coupled Majorana mode(s), we have to extend the Hilbert space by additional fermion state f (that can be either empty or occupied). We have numerically diagonalized the Hamiltonian (E1) in the representation $|n_{d\uparrow}\rangle \otimes |n_{d\downarrow}\rangle \otimes |n_f\rangle$, determining the eigenvalues and eigenvectors. Using the Lehmann representation we have computed the spectral functions $A_{\sigma}(\omega)$.

Figure 16 shows the QD spectrum for three representative values of the Coulomb potential. In the weak interaction limit (top panel) the spectrum exhibits the non-crossing Andreev quasiparticle branches coexisting with the zero-energy mode. For $U = \Gamma_S$, we observe a tendency towards avoided crossing of the Andreev bound states at $\xi_d \sim 0$ ($\epsilon \sim -\frac{U}{2}$). In the strong correlation case $U = 2\Gamma_S$ (bottom panel), there appear two such (avoided crossing) points aside from the half-filling [55]. In all cases there exist the zero-energy quasiparticle state, although its spectral weight is largest nearby these avoided-crossing points, corresponding to the quantum phase transition from the (spinfull) doublet to the (spinless) BCS-type configurations. This avoidance instead of true crossing is a hallmark of the states' hybridization with the Majorana mode [34, 78, 81].

Finally let us check, if the leaking Majorana mode can affect the opposite \downarrow spin of the proximitized correlated quantum dot. We compare the spectra of both spins in Fig. 17. To be specific, we focus on the weak correlation limit ($\Gamma_S \gg U$) when the pairing effects are most efficient. For $t_m = 0$, both spectra are obviously identical and they are characterized by two gapped Andreev quasiparticle branches. With increasing t_m , we observe signatures of the leaking Majorana mode in both spins, with dominance in \uparrow sector. Tiny feature of the zero-energy mode shows up in the spin \downarrow sector only near $\xi_d \sim 0$, where the on-dot pairing between both spins is the most efficient. Another difference between the spin-resolved spectra is observed at large couplings t_m , where a number of the Andreev branches doubles for \uparrow sector (due to the bonding/antibonding states formed in the 'molecular' limit [35]) whereas such effect is absent for \downarrow electrons.

[1] J. Alicea, "New directions in the pursuit of Majorana fermions in solid state systems," Rep. Prog. Phys. **75**, 076501 (2012).

[2] M. Leijnse and K. Flensberg, "Introduction to topological superconductivity and Majorana fermions," Semicond. Sci. Technol. **27**, 124003 (2012).

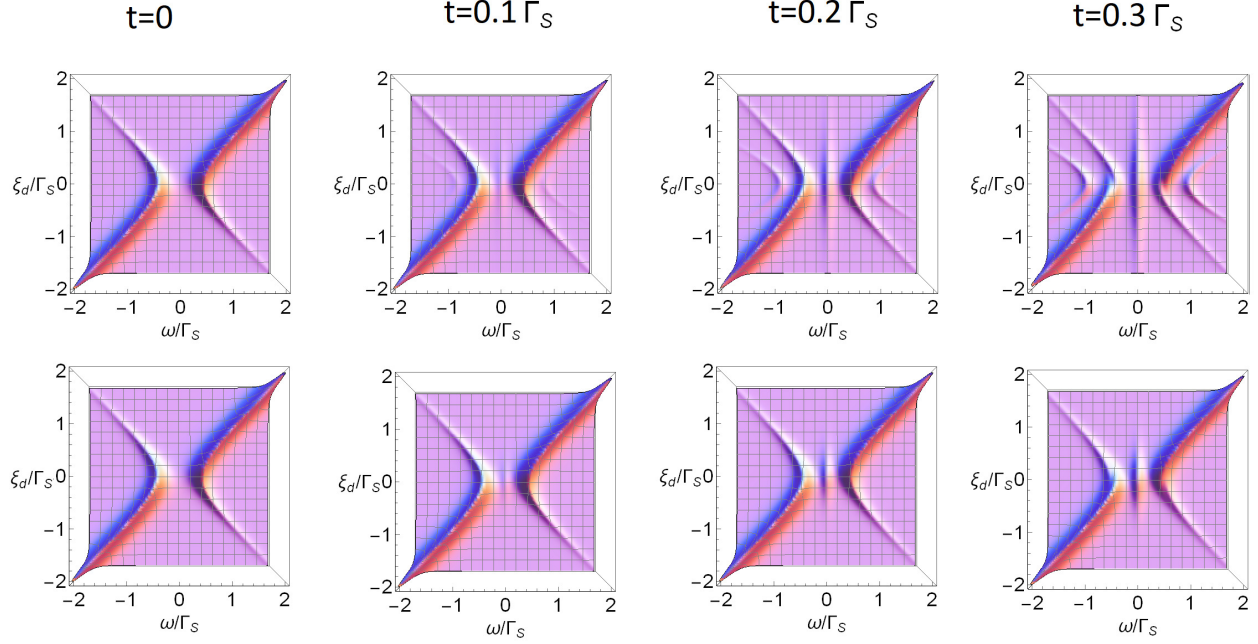


FIG. 17. Comparison of the spectral functions $A_\sigma(\omega)$ for \uparrow (upper row) and \downarrow electrons (bottom row) in the superconducting atomic limit obtained for $U/\Gamma_S = 0.05$, $\epsilon_m = 0$ and several couplings t_m (as indicated).

- [3] T. D. Stanescu and S. Tewari, “Majorana fermions in semiconductor nanowires: fundamentals, modeling, and experiment,” *J. Phys.: Condens. Matter* **25**, 233201 (2013).
- [4] C. W. J. Beenakker, “Search for Majorana fermions in superconductors,” *Annu. Rev. Condens. Matter Phys.* **4**, 113 (2013).
- [5] S. R. Elliott and M. Franz, “Colloquium: Majorana fermions in nuclear, particle, and solid-state physics,” *Rev. Mod. Phys.* **87**, 137 (2015).
- [6] R. Aguado, “Majorana quasiparticles in condensed matter,” *Riv. Nuovo Cimento* **040**, 523 (2017).
- [7] R.M. Lutchyn, E.P.A.M. Bakkers, L.P. Kouwenhoven, P. Krogstrup, C.M. Marcus, and Y. Oreg, “Realizing Majorana zero modes in superconductor-semiconductor heterostructures,” (2017), arXiv:1707.04899.
- [8] G. E. Volovik, “Fermion zero modes on vortices in chiral superconductors,” *JETP Lett.* **70**, 609 (1999).
- [9] N. Read and D. Green, “Paired states of fermions in two dimensions with breaking of parity and time-reversal symmetries and the fractional quantum Hall effect,” *Phys. Rev. B* **61**, 10267 (2000).
- [10] A. Y. Kitaev, “Unpaired Majorana fermions in quantum wires,” *Phys. Usp.* **44**, 131 (2001).
- [11] X. Liu, X. Li, D.-L. Deng, X.-J. Liu, and S. Das Sarma, “Majorana spintronics,” *Phys. Rev. B* **94**, 014511 (2016).
- [12] S. Tewari, S. Das Sarma, C. Nayak, C. Zhang, and P. Zoller, “Quantum computation using vortices and Majorana zero modes of a $p_x + ip_y$ superfluid of fermionic cold atoms,” *Phys. Rev. Lett.* **98**, 010506 (2007).
- [13] L. Fu and C. L. Kane, “Superconducting proximity effect and Majorana fermions at the surface of a topological insulator,” *Phys. Rev. Lett.* **100**, 096407 (2008).
- [14] J. Nilsson, A. R. Akhmerov, and C. W. J. Beenakker, “Splitting of a Cooper pair by a pair of Majorana bound states,” *Phys. Rev. Lett.* **101**, 120403 (2008).
- [15] M. Sato and S. Fujimoto, “Topological phases of noncentrosymmetric superconductors: Edge states, Majorana fermions, and non-Abelian statistics,” *Phys. Rev. B* **79**, 094504 (2009).
- [16] M. Wimmer, A. R. Akhmerov, M. V. Medvedyeva, J. Tworzydło, and C. W. J. Beenakker, “Majorana bound states without vortices in topological superconductors with electrostatic defects,” *Phys. Rev. Lett.* **105**, 046803 (2010).
- [17] J. D. Sau, R. M. Lutchyn, S. Tewari, and S. Das Sarma, “Generic new platform for topological quantum computation using semiconductor heterostructures,” *Phys. Rev. Lett.* **104**, 040502 (2010).
- [18] Y. Oreg, G. Refael, and F. von Oppen, “Helical liquids and Majorana bound states in quantum wires,” *Phys. Rev. Lett.* **105**, 177002 (2010).
- [19] R. M. Lutchyn, J. D. Sau, and S. Das Sarma, “Majorana fermions and a topological phase transition in semiconductor-superconductor heterostructures,” *Phys. Rev. Lett.* **105**, 077001 (2010).
- [20] T.-P. Choy, J. M. Edge, A. R. Akhmerov, and C. W. J. Beenakker, “Majorana fermions emerging from magnetic nanoparticles on a superconductor without spin-orbit coupling,” *Phys. Rev. B* **84**, 195442 (2011).
- [21] L. Jiang, T. Kitagawa, J. Alicea, A. R. Akhmerov, D. Pekker, G. Refael, J. I. Cirac, E. Demler, M. D. Lukin, and P. Zoller, “Majorana fermions in equilibrium and in driven cold-atom quantum wires,” *Phys. Rev. Lett.* **106**, 220402 (2011).
- [22] P. San-Jose, E. Prada, and R. Aguado, “ac Josephson effect in finite-length nanowire junctions with Majorana modes,” *Phys. Rev. Lett.* **108**, 257001 (2012).

- [23] V. Mourik, K. Zuo, S. M. Frolov, S. R. Plissard, E. P. A. M. Bakkers, and L. P. Kouwenhoven, “Signatures of Majorana fermions in hybrid superconductor-semiconductor nanowire devices,” *Science* **336**, 1003 (2012).
- [24] H. Zhang et al., “Ballistic Majorana nanowire devices,” (2016), arXiv:1603.04069.
- [25] S. Nadj-Perge, I. K. Drozdov, J. Li, H. Chen, S. Jeon, J. Seo, A. H. MacDonald, B. A. Bernevig, and A. Yazdani, “Observation of Majorana fermions in ferromagnetic atomic chains on a superconductor,” *Science* **346**, 602 (2014).
- [26] R. Pawlak, M. Kisiel, J. Klinovaja, T. Maier, S. Kawai, T. Glatzel, D. Loss, and E. Meyer, “Probing atomic structure and Majorana wave-functions in mono-atomic Fe-chains on superconducting Pb-surface,” *npj Quantum Info* **2**, 16035 (2016).
- [27] M. Ruby, F. Pientka, Y. Peng, F. von Oppen, B. W. Heinrich, and K. J. Franke, “End states and subgap structure in proximity-coupled chains of magnetic adatoms,” *Phys. Rev. Lett.* **115**, 197204 (2015).
- [28] S. Jeon, Y. Xie, J. Li, Z. Wang, B. A. Bernevig, and A. Yazdani, “Distinguishing a Majorana zero mode using spin-resolved measurements,” *Science* **358**, 772 (2017).
- [29] M. T. Deng, S. Vaitiekėnas, E. B. Hansen, J. Danon, M. Leijnse, K. Flensberg, J. Nygård, P. Krogstrup, and C. M. Marcus, “Majorana bound state in a coupled quantum-dot hybrid-nanowire system,” *Science* **354**, 1557 (2016).
- [30] E. Vernek, P. H. Penteado, A. C. Seridonio, and J. C. Egues, “Subtle leakage of a Majorana mode into a quantum dot,” *Phys. Rev. B* **89**, 165314 (2014).
- [31] C.-X. Liu, J. D. Sau, T. D. Stanescu, and S. Das Sarma, “Andreev bound states versus Majorana bound states in quantum dot-nanowire-superconductor hybrid structures: Trivial versus topological zero-bias conductance peaks,” *Phys. Rev. B* **96**, 075161 (2017).
- [32] S. Hoffman, D. Chevallier, D. Loss, and J. Klinovaja, “Spin-dependent coupling between quantum dots and topological quantum wires,” *Phys. Rev. B* **96**, 045440 (2017).
- [33] Andrzej Ptak, Aksel Kobińska, and Tadeusz Domański, “Controlling the bound states in a quantum-dot hybrid nanowire,” *Phys. Rev. B* **96**, 195430 (2017).
- [34] E. Prada, R. Aguado, and P. San-Jose, “Measuring Majorana nonlocality and spin structure with a quantum dot,” *Phys. Rev. B* **96**, 085418 (2017).
- [35] J. Barański, A. Kobińska, and T. Domański, “Spin-sensitive interference due to Majorana state on the interface between normal and superconducting leads,” *J. Phys.: Condens. Matter* **29**, 075603 (2017).
- [36] R. Chirila and C. P. Moca, “Fingerprints of Majorana fermions in spin-resolved subgap spectroscopy,” *Phys. Rev. B* **94**, 045405 (2016).
- [37] R. Žitko, J. Soo Lim, R. López, and R. Aguado, “Shiba states and zero-bias anomalies in the hybrid normal-superconductor Anderson model,” *Phys. Rev. B* **91**, 045441 (2015).
- [38] T. Domański, I. Weymann, M. Barańska, and G. Górski, “Constructive influence of the induced electron pairing on the Kondo state,” *Sci. Rep.* **6**, 23336 (2016).
- [39] E. J. H. Lee, X. Jiang, R. Žitko, R. Aguado, C. M. Lieber, and S. De Franceschi, “Scaling of subgap excitations in a superconductor-semiconductor nanowire quantum dot,” *Phys. Rev. B* **95**, 180502 (2017).
- [40] D. E. Liu and H. U. Baranger, “Detecting a Majorana-fermion zero mode using a quantum dot,” *Phys. Rev. B* **84**, 201308 (2011).
- [41] R. López, M. Lee, L. Serra, and J. S. Lim, “Thermoelectrical detection of Majorana states,” *Phys. Rev. B* **89**, 205418 (2014).
- [42] M. Lee, J. S. Lim, and R. López, “Kondo effect in a quantum dot side-coupled to a topological superconductor,” *Phys. Rev. B* **87**, 241402 (2013).
- [43] Y. Cao, P. Wang, G. Xiong, M. Gong, and X.-Q. Li, “Probing the existence and dynamics of Majorana fermion via transport through a quantum dot,” *Phys. Rev. B* **86**, 115311 (2012).
- [44] W.-J. Gong, S.-F. Zhang, Z.-C. Li, G. Yi, and Y.-S. Zheng, “Detection of a Majorana fermion zero mode by a T-shaped quantum-dot structure,” *Phys. Rev. B* **89**, 245413 (2014).
- [45] D. E. Liu, M. Cheng, and R. M. Lutchyn, “Probing Majorana physics in quantum-dot shot-noise experiments,” *Phys. Rev. B* **91**, 081405 (2015).
- [46] P. Stefański, “Signatures of Majorana states in electron transport through a quantum dot coupled to topological wire,” *Acta Phys. Pol. A* **127**, 198 (2015).
- [47] Z.-Z. Li, C.-H. Lam, and J. Q. You, “Probing Majorana bound states via counting statistics of a single electron transistor,” *Sci. Rep.* **5**, 11416 (2015).
- [48] I. Weymann, “Spin Seebeck effect in quantum dot side-coupled to topological superconductor,” *J. Phys.: Condens. Matter* **29**, 095301 (2017).
- [49] I. Weymann and K. P. Wójcik, “Transport properties of a hybrid Majorana wire-quantum dot system with ferromagnetic contacts,” *Phys. Rev. B* **95**, 155427 (2017).
- [50] S.-X. Wang, Y.-X. Li, N. Wang, and J.-J. Liu, “Andreev reflection in a T-shaped double quantum-dot with coupled Majorana bound states,” *Acta Phys. Sin.* **65**, 137302 (2016).
- [51] A. V. Balatsky, I. Vekhter, and J.-X. Zhu, “Impurity-induced states in conventional and unconventional superconductors,” *Rev. Mod. Phys.* **78**, 373 (2006).
- [52] T. Domański, “Particle-hole mixing driven by the superconducting fluctuations,” *Eur. Phys. J. B* **74**, 437 (2010).
- [53] A. Golub, “Multiple Andreev reflections in *s*-wave superconductor-quantum dot-topological superconductor tunnel junctions and Majorana bound states,” *Phys. Rev. B* **91**, 205105 (2015).
- [54] D. A. Ruiz-Tijerina, E. Vernek, L. G. G. V. Dias da Silva, and J. C. Egues, “Interaction effects on a Majorana zero mode leaking into a quantum dot,” *Phys. Rev. B* **91**, 115435 (2015).
- [55] J. Bauer, A. Oguri, and A. C. Hewson, “Spectral properties of locally correlated electrons in a Bardeen-Cooper-Schrieffer superconductor,” *J. Phys.: Condens. Matter* **19**, 486211 (2007).
- [56] Y. Yamada, Y. Tanaka, and N. Kawakami, “Interplay of Kondo and superconducting correlations in the nonequilibrium Andreev transport through a quantum dot,” *Phys. Rev. B* **84**, 075484 (2011).
- [57] A. Martín-Rodero and A. Levy Yeyati, “Josephson and Andreev transport through quantum dots,” *Advances in Physics* **60**, 899 (2011).
- [58] J. Barański and T. Domański, “In-gap states of a quantum dot coupled between a normal and a superconducting lead,” *J. Phys.: Condens. Matter* **25**, 435305 (2013).

- [59] A. F. Andreev, “The thermal conductivity of the intermediate state in superconductors.” *J. Exp. Theor. Phys* **19**, 1228 (1964).
- [60] M. Krawiec and K.I. Wysokiński, “Electron transport through a strongly interacting quantum dot coupled to a normal metal and BCS superconductor,” *Supercond. Sci. Technol.* **17**, 103 (2004).
- [61] A. Schuray, L. Weithofer, and P. Recher, “Fano resonances in Majorana bound states-quantum dot hybrid systems,” *Phys. Rev. B* **96**, 085417 (2017).
- [62] M. Cheng, M. Becker, B. Bauer, and R. M. Lutchyn, “Interplay between Kondo and Majorana interactions in quantum dots,” *Phys. Rev. X* **4**, 031051 (2014).
- [63] I. J. van Beek and B. Braunecker, “Non-Kondo many-body physics in a Majorana-based Kondo type system,” *Phys. Rev. B* **94**, 115416 (2016).
- [64] Y. Tanaka, N. Kawakami, and A. Oguri, “Numerical renormalization group approach to a quantum dot coupled to normal and superconducting leads,” *J. Phys. Soc. Japan* **76**, 074701 (2007).
- [65] T. Domański, M. Žonda, V. Pokorný, G. Górski, V. Janiš, and T. Novotný, “Josephson-phase-controlled interplay between correlation effects and electron pairing in a three-terminal nanostructure,” *Phys. Rev. B* **95**, 045104 (2017).
- [66] E. Vecino, A. Martín-Rodero, and A. Levy Yeyati, “Josephson current through a correlated quantum level: Andreev states and π junction behavior,” *Phys. Rev. B* **68**, 035105 (2003).
- [67] K. G. Wilson, “The renormalization group: Critical phenomena and the Kondo problem,” *Rev. Mod. Phys.* **47**, 773–840 (1975).
- [68] O. Legeza, C. P. Moca, A. I. Toth, I. Weymann, and G. Zarand, “Manual for the Flexible DM-NRG code,” (2008), arXiv:0809.3143.
- [69] W. C. Oliveira and Luiz N. Oliveira, “Generalized numerical renormalization-group method to calculate the thermodynamical properties of impurities in metals,” *Phys. Rev. B* **49**, 11986–11994 (1994).
- [70] G. Górski, “Irreducible Green functions method applied to nanoscopic systems,” *Acta Phys. Pol.* **130**, 551 (2016).
- [71] J. J. He, T. K. Ng, P. A. Lee, and K. T. Law, “Selective equal-spin Andreev reflections induced by Majorana fermions,” *Phys. Rev. Lett.* **112**, 037001 (2014).
- [72] A. Haim, E. Berg, F. von Oppen, and Y. Oreg, “Signatures of Majorana zero modes in spin-resolved current correlations,” *Phys. Rev. Lett.* **114**, 166406 (2015).
- [73] C. Ren, J. Yang, J. Xiang, S. Wang, and H. Tian, “Non-local spin blocking effect of zero-energy Majorana fermions,” *Journal of the Physical Society of Japan* **86**, 124715 (2017), <https://doi.org/10.7566/JPSJ.86.124715>.
- [74] B. Béri and N. R. Cooper, “Topological kondo effect with majorana fermions,” *Phys. Rev. Lett.* **109**, 156803 (2012).
- [75] M. R. Galpin, A. K. Mitchell, J. Temaismithi, D. E. Logan, B. Béri, and N. R. Cooper, “Conductance fingerprint of majorana fermions in the topological kondo effect,” *Phys. Rev. B* **89**, 045143 (2014).
- [76] S. Plugge, A. Zazunov, E. Eriksson, A. M. Tsvelik, and R. Egger, “Kondo physics from quasiparticle poisoning in majorana devices,” *Phys. Rev. B* **93**, 104524 (2016).
- [77] B. Béri, “Exact nonequilibrium transport in the topological kondo effect,” *Phys. Rev. Lett.* **119**, 027701 (2017).
- [78] M. T. Deng, S. Vaitiekėnas, E. Prada, P. San-Jose, J. Nygård, P. Krogstrup, R. Aguado, and C. M. Marcus, “Majorana non-locality in hybrid nanowires,” (2017), arXiv:1712.03536.
- [79] D. Chevallier, P. Simon, and C. Bena, “From Andreev bound states to Majorana fermions in topological wires on superconducting substrates: A story of mutation,” *Phys. Rev. B* **88**, 165401 (2013).
- [80] D. Rainis, L. Trifunovic, J. Klinovaja, and D. Loss, “Towards a realistic transport modeling in a superconducting nanowire with Majorana fermions,” *Phys. Rev. B* **87**, 024515 (2013).
- [81] D. Chevallier, P. Szumniak, S. Hoffman, D. Loss, and J. Klinovaja, “Topological phase detection in Rashba nanowires with a quantum dot,” *Phys. Rev. B* **97**, 045404 (2018).
- [82] M. M. Maška and T. Domański, “Polarization of the Majorana quasiparticles in the Rashba chain,” *Sci. Rep.* **7**, 16193 (2017).
- [83] A. Martín-Rodero and A. Levy Yeyati, “The Andreev states of a superconducting quantum dot: mean field versus exact numerical results,” *J. Phys.: Condens. Matter* **24**, 385303 (2012).